MAGIC sensitivity to Primordial Black Hole bursts and modelization of BH chromospheres and gamma-ray emission spectra

MASTER IN HIGH ENERGY PHYSICS,
ASTROPHYSICS AND COSMOLOGY

Master thesis
September 2015

Author:
Miquel CASSANYES

Supervisors:
Dr. Javier RICO
Dr. Oriol PUJOLÀS

Contents

1 Introduction

1.1 The goals of this work

Primordial black holes (PBHs) are black holes (BHs) formed in the early Universe, which exhibit a very wide range of possible initial masses depending on when and how they were formed. BHs are expected to radiate particles, process in which their mass is reduced over time and their temperature increases. The end of this time evolution is thought to be an explosion at extremely large temperatures resulting in a short burst of very high energy particles.

Given that the temperature of a black hole will always increase over time (and it will also increase faster over time), it comes naturally to ask what will happen when a BH reaches temperatures beyond Λ_{QCD}, because a black hole is expected to radiate quarks and gluons rather than hadronic matter, at such temperatures. The existence of chromospheres surrounding black holes is a topic of discussion nowadays, especially since the recent observation of jet-quenching in heavy ion collisions, that suggests an overestimation of the number of hard jets that pass through a quark gluon plasma. The presence or absence of chromospheres is key to predict the emission spectra of black holes, because a chromosphere would significantly soften any hard jet that could be emitted and hence suppress the emission at very high energies.

In the last stages of a black hole's life, its temperature is high enough for gamma-rays to be emitted. For this reason, Cherenkov telescopes, and in particular MAGIC, might be able to detect this radiation, which would appear as a flare lasting for a few minutes. Such an event would present a series of features that would allow to distinguish between it and a gamma-ray burst, like, for instance, a soft-to-hard evolution instead of the hard-to-soft one that gamma-ray bursts exhibit. However, the existance of a chromosphere surrounding the black hole might soften the spectrum so much that the very high energies required for a MAGIC detection are not reached.

In this work, I have approached two of the most important facets involved in the search for PBHs, namely the determination of the expected particle spectrum and the perspectives for detection with the present and future gamma-ray instruments. On the one hand, I have developed a toy model for black hole chromospheres that represents an extreme possibility that allows the determination of the systematic errors of models of PBH surroundings, rather than attempting to provide a realistic explanation. This model is based on the assumption that the quark-gluon plasma can be treated as an ultrarelativistic perfect fluid at thermal equilibrium and hence the black hole emission spectrum is expected to show a thermal profile. In the second part of this work, we estimate the MAGIC sensitivity to primordial black hole bursts by calculating the minimum detectable burst rate density. To do so, we adapt a method originally applied to Milagro and HAWC for MAGIC and afterwards we compare our results to theirs. As a final comment, we briefly discuss how CTA could perform in comparison to MAGIC and the other facilities. Despite having approached two major questions of this field, we have also seen that it is a very rich topic that provides lots of possible ways to carry out a continuation of this work.

1.2 General Relativity and black holes

To model black holes, we will use General Relativity (GR), given the tools it provides to describe such objects. We consider a space-time with a Minkowski metric, given by

$$ds^2 = -\left(1 - \frac{2GM_{BH}}{rc^2}\right)c^2dt^2 + \frac{dr^2}{1 - \frac{2GM_{BH}}{rc^2}} + r^2\left(d\theta^2 + d\phi^2\sin^2\theta\right). \tag{1}$$

where G is the gravitational constant, M_{BH} is the mass of the BH, c is the speed of light in vacuum and t, r, θ and ϕ are the coordinates we use, which correspond to time and the standard tridimensional spherical coordinates, respectively.

A black hole is an object of classical gravity contained within a volume of radius

$$r_{BH} = \frac{2GM_{BH}}{c^2}. \tag{2}$$

We assume no rotation nor electric charge.

Notice the importance of M_{BH}, that fixes the BH radius and, as we will see, its temperature and lifetime too. A natural question, then, arises, to know if there is any limitation in the mass range of a BH.

From Equation 2, we can see that $\rho_{BH} \propto M_{BH}^{-2}$. For this reason, we would expect BHs not to be homogeneously distributed with respect to their mass, because the density required for a certain BH to form will strongly depend on the matter density of the Universe. Moreover, the density of matter in the Universe has evolved with time and hence it is much more difficult for a small-mass BH to form in the recent history of the Universe, where ρ_m is smaller, than in priomordial times when this density was larger.

Primordial Black Holes are BHs formed in the early Universe (i.e. before the formation of the first stars). Several formation mechanisms are being considered, including the collapse of overdense regions arising from priomordial inhomogeneities, like those expected in inflationary models, for example, or cosmological phase transitions, among others.

It is thought that the range of possible PBH initial masses is enormous. The relation between the initial mass and the formation time of the PBH, given by $M_{BH} \approx 10^5(t/10^{-23}\ \mathrm{s})\ g$, shows that the wide interval of possible initial times (i.e. from the Plank time to the time of formation of the first stars, roughly) leads to an initial mass interval that goes from the Planck mass to $\sim 10^5 M_\odot$.

Several studies have found constraints in the number of PBHs within a certain mass range as well as upper limits on the background distribution of PBHs of certain masses. These results are based on phenomena that are expected to be related to or affected by PBHs, namely primordial nucleosynthesis, CMB anisotropies, MACHO searches and the search for Hawking radiation. There are also groups trying to observe the gamma-ray burst of Hawking radiation produced by an expiring PBH to directly constraint the local number

PBH mass	PBH temperature
$1\ M_{\odot} \simeq 1.99 \times 10^{33}$ g	10^{-7} K
10^{25} g	2.7 K
10^{11} g	100 GeV$\simeq 1.23 \times 10^{15}$ K

Table 1: Some PBH masses and their respective Hawking temperatures.

density of PBH of mass $M_{BH} \approx 5 \times 10^{14}$ g and larger, because given their formation times and thermodynamic evolution, they are expected not to have expired yet.

As we mentioned before, the mass of a BH defines its temperature. Thanks to the work by Hawking and Beckenstein, classical thermodynamical theories were extended to include BHs, where the so-called Hawking (Gravitational) temperature was presented as

$$kT_{BH} = \frac{\hbar c^3}{8\pi G M_{BH}} = 1.06 \left(\frac{M_{BH}}{10^{13}\ g} \right)^{-1} GeV \tag{3}$$

where k and $\hbar$ are the Boltzmann and reduced Planck constants. Table 1 shows a few examples of BH masses and temperatures.

Moreover, as suggested by Hawking, a BH is expected to radiate particles. The emitted particles are those that seem non-composite when compared with the wavelength that corresponds to the BH temperature T_{BH}. This indicates that, at sufficiently large temperatures, a BH should directly emit quarks, gluons, leptons and photons (this would happen at $T_{BH} \geq \Lambda_{QCD} \approx 200$ MeV). After being ejected, quarks and gluons would interact and hadronize when the temperature was below this Λ_{QCD} threshold becoming stable species.

This radiative process causes the BH to lose mass over time. Therefore, every BH has a remaining lifetime that depends on its mass as

$$\tau \sim \frac{G^2 M^3}{\hbar c^4}. \tag{4}$$

Given the relationship between M_{BH} and T_{BH}, we can express the temperature of a BH as a function of its remaining lifetime as

$$T_{BH} \sim \left(\frac{\hbar^2 c^5}{8^3 \pi^3 G k^3} \frac{1}{\tau} \right)^{1/3}. \tag{5}$$

Notice that, the shorter the remaining lifetime of a BH, the higher its temperature. Considering that the mass loss goes as $\dot{M} \sim T_{BH}^2$, a higher temperature will cause the BH to emit more rapidly, which will cause it to reduce its mass and hence also its lifetime and, as a result, to increase its temperature. This process will eventually lead to a massive explosion after the BH has reached arbitrarily large temperatures (see Figure 1). Take into account, then, that the Hawking-radiated particles will also exhibit extremely large energies.

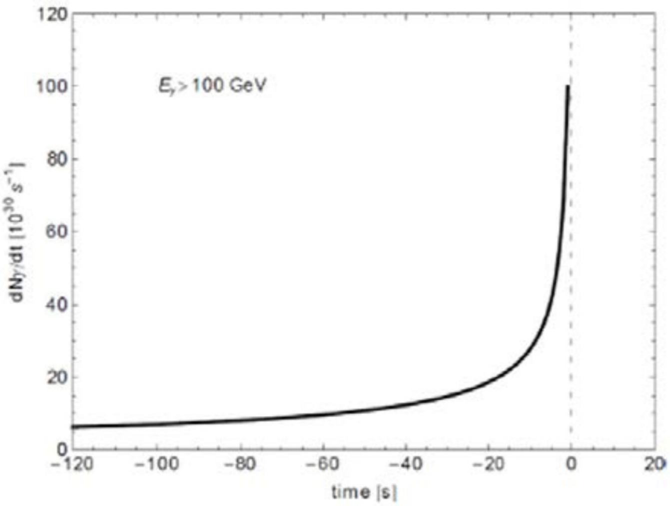

Figure 1: *Calculation for the PBH burst light curve dN/dt arriving in the detector with energy above a threshold of 100 GeV (plot from [MacGibbon (2014)]).*

1.3 The MAGIC telescopes

The MAGIC telescopes are two Imaging Atmospheric Cherenkov Telescopes (IACTs) designed to cover the range between 50 GeV and 50 TeV in the electromagnetic spectrum with optical dishes of 17 m in diameter separated by 85 m located roughly 2200 m above the sea level at the Observatorio del Roque de los Muchachos (ORM)[1] on the Canarian island of La Palma (28°45'25"N 17°53'33"W). The first one, MAGIC I, was installed in 2004 and MAGIC II is operating since 2009 providing data in stereoscopic mode together with MAGIC I.

Both telescopes have their mirrors supported by carbon fiber reinforced plastic tubes, which form a solid and light-weighted structure that makes it possible to reorient the telescopes in a few tens of seconds to record data in case of a gamma-ray burst (GRB) alert from satellite detectors. The mirrors are composed of panels, each one having a spherical shape, but assembled together in a parabolic one. The focal length of both telescopes is 17 m. Their cameras consist of 1039 photomultiplier tubes (PMTs) each with a peak in quantum efficiency of 32% at around 330 nm wavelength. In addition, light guides cover the spaces between the surfaces covered by PMTs to improve the sensitivity in these areas. The electrical signal of the PMTs is amplified before being transformed into an optical signal and being sent to the counting house. In the counting house, the trigger system detects air-shower events and, in case one is spotted, stores the data.

Since the MAGIC telescopes are ground-based, the atmosphere plays a crucial role in their detection principle. When a gamma-ray enters the atmosphere, it most likely interacts with another particle, creating an electron-positron pair. These particles will also interact with other particles within the atmosphere, emitting gamma rays through bremsstrahlung,

[1] `http://www.iac.es/eno.php?op1=2&lang=en`

Figure 2: *The telescopes MAGIC I and MAGIC II in La Palma.*

which produce new e^+e^- pairs, resulting in a particle cascade called air-shower, where most of the particles descend in a narrow cone. These particles are faster than light in the medium and, therefore, Cherenkov radiation is emitted. This radiation is bluish and it is what we observe with the MAGIC telescopes.

The MAGIC cameras collect the Cherenkov light and, using information such as the total amount of light, the shape of the image and its position and orientation, one can reconstruct the air-shower and obtain information about the primary particle, such as its incident direction, energy and particle identification. It is important to know that gamma-rays are not the only particles that can initiate an air-shower. Electrons, positrons and hadrons (mainly protons and Helium nuclei) can also start them and they actually dominate the trigger rate of Cherenkov telescopes, but, fortunately, there are ways to distinguish between the different types, at least to some extent [Hillas (1985), Hillas (2013), Weekes (1989)]. As we will see in Section 3.1, the rate of irreducible background is one of the quantities determining the sensitivity of MAGIC to detect gamma-ray sources in general and, in particular, BH bursts.

The MAGIC telescopes can only operate at night due to the extreme sensitivity of their cameras. On top of that, good atmospherical conditions are required to collect useful data, because the gamma-ray detection depends on Cherenkov light air-showers produced in the atmosphere, which gets absorbed by clouds or impurities within it. These two aspects con-

BH bursts	**Other known GRBs**
Local, unlikely to be detected from beyond the Galaxy.	Detected at cosmological distances.
Soft-to-hard evolution expected.	Most GRBs show hard-to-soft evolution.
Accompanied by hadronic bursts which may be detectable if local.	Hadrons not expected from GRBs.
No accompanying gravitational wave signal.	Gravitational wave signal expected.
Time duration of bursts most likely around 1-100 seconds.	Time duration ranges from fractions of second to hours.
Exponential Rise Fast Fall (ERFF) light curve.	Fast Rise Exponential Decay (FRED) light curve.
No multi-wavelength photon afterglows unless in exotic environment.	X-ray, optical, radio afterglows expected.
TeV spectra predicted.	TeV emission unknown.
Single-peak time profile.	Multi-peak time profile.
No burst repetition.	May be repeating.

Table 2: *Main differences between BH burst and GRBs.*

siderably reduce the observational time of the telescopes to about 1000 h per year. Their field of view (FOV) is rather narrow, with an effective radius of about 1°, so they point towards possible sources of interest to be able to detect them. However, given their angular resolution of 0.1-0.2°, depending on the energy, the FOV appears to be empty for most of the data, even when a point gamma-ray source is detected. Then, a large fraction of the total MAGIC data could be useful to carry out a PBH search.

As previously stated, MAGIC covers an energy range that goes from 50 GeV to 50 TeV. Even though these values are quite large, in the final stages of a BH lifetime, these energies (and beyond) should be reached by their emitted gamma-rays. Then, as far as energy range goes, the detection of PBHs with MAGIC would make sense.

Apart from energy range, other issues need to be taken into account when considering if PBH detections are possible with MAGIC. A key aspect is to be able to distinguish a BH burst from GRBs and, in that regard, it is particularly important to remark the soft-to-hard time evolution, which is the opposite situation to other sources. Table 2 shows this one and other differences between how we expect BH bursts to be and expectations of other GRBs [MacGibbon (2014)]. We see that there a several features we can use to distinguish PBH bursts from other events. In some cases the observation of an event with certain properties would be remarkable enough, even if the source was not a PBH. That would be the case, for example, of a short burst with such high energy, which has never been observed.

Here we perform a study of how to best use the capabilities of the MAGIC telescopes to detect bursts from evaporating BHs, estimating their sensitivity to PBH bursts based on technical and performance properties of the facility.

2 Modeling PBHs with chromosphere

Since the main signature from PBHs comes from its final super-hot evaporation burst, the theoretical modeling of the PBHs inevitably requires a substantial amount of complicated QCD phenomena such as the hadronization of the primary quarks and gluons emitted by BHs. These phenomena are usually modeled with jet algorithms, and even in the absence of the BHs it is not easy to estimate the systematic errors associated with them.

For instance, the recent observation of the so-called jet-quenching in heavy ion collisions indicates that jet algorithms might overestimate (by even a factor 5) the number of hard jets that pass through a quark-gluon plasma environment. This motivates a revision of the chromosphere formation which is not based on jet algorithms.

Therefore, we aim to provide a simple model that can be taken as an extreme possibility that serves not as a realistic model of the PBH surroundings but as a way to estimate the systematic errors made in its theoretical modeling. In this chapter, we will first check that this model describes a physically possible chromosphere, we will then discuss the emission spectrum related to our chromosphere and, as a final comment, we will present the constraint for Ω_{PBH} that can be deduced from our model.

2.1 PBH chromosphere toy model

The brief scheme of our model that is presented above suggests that there will be a spherically-shaped region surrounding the BH enclosing a quark-gluon plasma with temperatures above Λ_{QCD}. The existance of this plasma is a matter of discussion when it comes to PBH models and we will assume that it is present because of similarities between the environment surrounding a PBH and recent heavy-ion experiments at LHC, which suggest a significant softening of the jets that are emitted that can be associated with the strong interaction of the particles involved [Aamodt (2011), d'Enterria (2005)].

The region where we find this plasma is defined by two radii. The first one is the innermost one (i.e. closest to the BH singularity) and corresponds to the region where particles are injected into the plasma. What really happens is that, at the horizon of the BH, particles are Hawking-radiated and, shortly afterwards, interact becoming part of the plasma, but we can treat that as particles being injected into an already existing plasma in a simplified scenario. The second radius corresponds to the region where the plasma hadronizes. That happens when $T \leq \Lambda_{QCD}$, roughly, so we can use that to determine r_Λ.

Let us consider that particles are injected into the plasma at temperature $T_i \gg \Lambda_{QCD}$. The power emitted by the BH is assumed to be fully transmited to the plasma at r_{BH} and fully re-emitted by the plasma at r_Λ, so

$$\begin{aligned} \dot{M} \sim T_i^2 \sim r_\Lambda^2 \Lambda_{QCD}^4 \\ r_\Lambda \sim \frac{T_i}{\Lambda_{QCD}^2} \end{aligned} \tag{6}$$

Notice that $r_\Lambda \sim \frac{T_i^2}{\Lambda^2}\frac{1}{T_i} \gg \frac{1}{T_i} \sim r_{BH}$, as we should expect.

For the sake of simplicity, we will assume that particles are within the Standard Model of Physics and that, when the plasma hadronizes, the full reemission power is invested in photons.

We will now describe our basic consistency check for this model. As we have mentioned before, we have assumed that the quark-gluon plasma can be treated as a perfect fluid, so we can express it in terms of its stress-energy tensor as

$$T_{\mu\nu} = \rho u_\mu u_\nu + P(g_{\mu\nu} + u_\mu u_\nu) = (\rho + P)u_\mu u_\nu + P g_{\mu\nu} \tag{7}$$

where ρ and P are the density and the pressure of the fluid, respectively, and u is the velocity four-vector. It is important to remark that we considered a Schwarzschild metric at the beginning (see Equation 1), but given that we focus on PBHs with masses around 5×10^{14} g, which are considered to be expiring at the current epoch in the lifetime of the Universe, $1-\frac{2GM_{BH}}{rc^2} \approx 1$ and hence we can work in Minkowski space. We will use spherical coordinates and, in this case, the metric can be written as

$$ds^2 = -c^2dt^2 + dx^2 + r^2\left(d\theta^2 + d\phi^2\sin^2\theta\right) \tag{8}$$

or, in matrix notation,

$$g = \begin{pmatrix} -1 & 0 & 0 & 0 \\ 0 & 1 & 0 & 0 \\ 0 & 0 & r^2 & 0 \\ 0 & 0 & 0 & r^2\sin^2\theta \end{pmatrix}. \tag{9}$$

Using the covariant derivate, we can express the conservation of the stress-energy tensor as

$$\nabla_\mu T^{\mu\nu} = 0. \tag{10}$$

From that expression, we can extract the two following equations.

$$0 = \partial_\mu T^{\mu 0} = \partial_0 T^{00} + \partial_i T^{i0} = \partial_0\left[(\rho+P)\gamma^2 - P\right] + \partial_i\left[(\rho+P)u^i u^0 + P\delta^{i0}\right] \tag{11}$$
$$0 = \partial_\mu T^{\mu i} = \partial_0 T^{0i} + \partial_j T^{ji} = \partial_0\left[(\rho+P)u^0 u^i + P\delta^{0i}\right] + \partial_j\left[(\rho+P)u^j u^i + P\delta^{ji}\right] \tag{12}$$

We have assumed an equation of state written as $P = w\rho$ for this fluid, so we can relate Equation 11 and Equation 12 more easily. We have also assumed that particles are ejected in radial direction from the plasma, so that $u = (\sqrt{1+u_r^2}, u_r, 0, 0)$ After some algebraic manipulation, we can find expressions for $\partial_r u_r$ and $\partial_r\rho$. They are given by

$$\partial_r u_r(r) = -\frac{2wu_r(r)(1+u_r^2(r))}{r(w+(-1+w)u_r^2(r))} \approx -\frac{2wu_r^3(r)}{r(-1+w)u_r^2(r)} \tag{13}$$
$$\partial_r\rho(r) = \frac{2(1+w)u_r^2(r)\rho(r)}{r(w+(-1+w)u_r^2(r))} \approx \frac{2(1+w)u_r^2(r)\rho(r)}{r(-1+w)u_r^2(r)} \tag{14}$$

where the approximations come from the fact that we can assume to be in the ultrarelativistic regime, where $u \gg 1$ because we are considering temperatures above Λ_{QCD} and particles have much larger velocities than rest masses. With this simplification, we can solve this system of differential equations, finding

$$u_r(r) \propto r^{\frac{2w}{1-w}} \tag{15}$$

$$\rho(r) \propto r^{\frac{2(1+w)}{-1+w}}. \tag{16}$$

If we also assume that this ultrarelativistic perfect fluid has an equation of state similar to that of radiation, which should be approximately the case for ultrarelativistic matter, i.e. $w \sim \frac{1}{3}$, substitution in the previous equations for u_r and ρ leads to

$$u_r(r) \propto r \tag{17}$$

$$\rho(r) \propto r^{-4}. \tag{18}$$

We do know that in the relativistic regime the energy density scales as T^4. Then, since $r \sim T^{-1}$, we should not be surprised to find that $\rho(r) \propto r^{-4}$. To understand why $u_r(r) \propto r$, we need to keep in mind that we expect the integrated energy flux over a spherical shell to be independent of r. That means that the energy flux should present an r^{-2} dependence. This flux can be written as $\Phi = \rho\gamma u_r^2$, so the only option for the integrated energy flux to be r-independent is indeed that $u_r(r) \propto r$.

This check allows us to see that the treatment of the quark-gluon plasma as a fluid exhibits a plausible behaviour, i.e. even if the plasma does not exactly behave like that, this would be a physically possible description if it did.

2.2 Emission spectrum toy model

So far, we have explained that we assume that a BH of mass M_{BH} Hawking-radiates Standard Model particles at its horizon distance r_{BH}, where the temperature is $T_i \geq \Lambda_{QCD}$. These particles move outwards in radial direction and form a quark-gluon plasma that can be described as an ultrarelativistic perfect fluid. Finally, they are reemited at r_Λ where the temperature is about Λ_{QCD} and hence hadronization takes place.

In addition to these assumptions, we will also assume that the quark-gluon plasma is at equilibrium, meaning that the total radiated power injected into it at r_{BH} is ejected at r_Λ. Not only that, but for simplification, we will also assume that the total ejected power is invested in the emission of photons, which is overly optimistic, but should serve us well for the toy model we are presenting.

The emission rate of such a BH can be written as [Carr et al. (2010)]

$$\frac{d^2N_s}{dEdt} = \frac{1}{2\pi}\frac{\Gamma_s}{e^{E/T_{BH}} - (-1)^{2s}} \tag{19}$$

where s is the spin of the emitted particle species, N_s is the number of spin s particles emitted, E their energy, T_{BH} their temperature, t the time and Γ_s is the dimensionless absorpotion coefficient, which is proportional to the cross-section σ_s. More precisely [Page (1976)],

$$\Gamma_s(M,E) = \frac{E^2\sigma_s(M,E)}{\pi} \tag{20}$$

where M stands for mass.

To be able to use these expressions, we need to determine the cross-sections for the different spin values. In [Page (1976)] we can see that

$$\sigma_{1/2}(M,E) = \begin{cases} 2\pi G^2M^2/c^4 & \text{for low } E \\ 27\pi G^2M^2/c^4 & \text{for high } E \end{cases} \tag{21}$$

$$\sigma_1(M,E) = \begin{cases} \frac{4}{3}AG^2M^2/c^4 \cdot E^2 & \text{for low } E \\ 27\pi G^2M^2/c^4 & \text{for high } E \end{cases} \tag{22}$$

where A is the surface area. To extend these expressions to analytical ones we can evaluate as function of the energy E, we can do the following. Let us assume a general case, with

$$\sigma_s(M,E) = \begin{cases} aM^{m_a}E^{e_a} & \text{for } E \ll E_* \\ bM^{m_b}E^{e_b} & \text{for } E \gg E_* \end{cases} \tag{23}$$

with m_i, e_i being certain integers that express the dependence of σ_s on M and E, a anb b being two constant values and E_* being the value the separtes the regime for low energies from that for high energies. Notice that

$$\sigma_s(M,E) = \frac{aM^{m_a}E^{e_a}}{2}(1-\tanh((E-E_*)c_a)) + \frac{bM^{m_b}E^{e_b}}{2}(1+\tanh((E-E_*)c_b)), \tag{24}$$

where c_i are parameters that adjust the softness of the change of behaviour from the low energy regime to the high energy one, fulfils the requirements set for both regimes, with a behavior near E_* described by the softness parameters c_i. That is so because for $E \ll E_*$, $\tanh((E-E_*)c_i) \approx -1$ and hence the first term becomes $aM^{m_a}E^{e_a}$ while the second one vanishes. For $E \gg E_*$, the opposite thing takes place, because $\tanh((E-E_*)c_i) \approx 1$.

Figure 3 shows the analytical functions we have used as $\sigma_{1/2}$ and σ_1, setting the softness parameters c_i to values that made the spectrum (we will discuss that later) have a reasonable dependence on E. We see that there is an intermediate region where the functions do not take any of the extreme values. We have set the softness parameters c_i so that the change of behavior was as quick as possible without disturbing the spectrum profile.

Regarding the regime separating point, E_*, we have used the values corresponding to the expected peaks of the spectrum for every particle species [Carr et al. (2010)]), because we would expect the change of regime to take place around the peak.

To be able to compare to other results, namely those of Carr. et al., we have considered a BH with intital temperature $T_i = 1$ GeV. They expect a large fraction of the photons that are finally emitted to come from π_0 annihilation processes and hence assume that the final reemission spectrum is peaked around $m_{\pi_0}/2 \simeq 68$ MeV. We have used the same assumption.

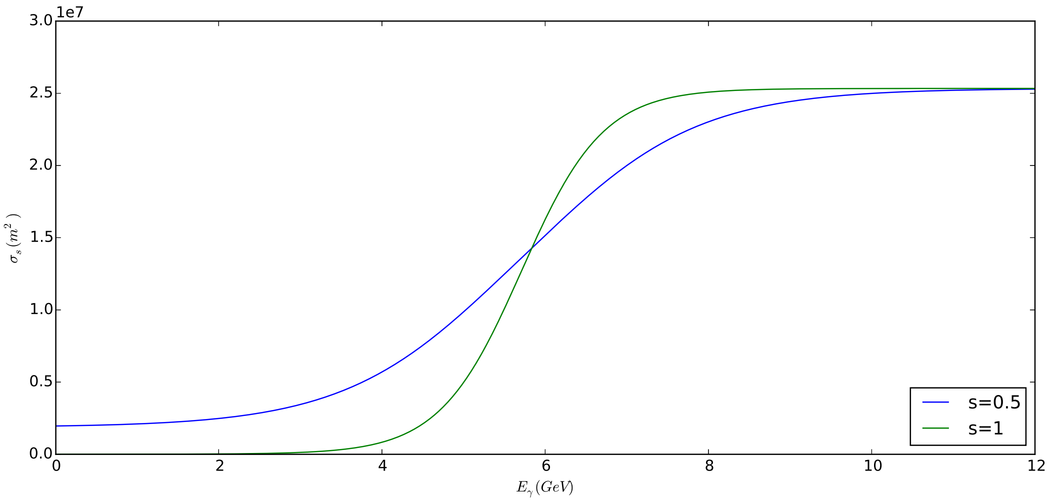

Figure 3: *Analytical functions used as $\sigma_{1/2}$ and σ_1 in our calculations as a function of photon energy E_γ.*

That means that in our final reemission spectrum, corresponding to the ejection of photons from the plasma, we consider contributions to the total emission power from the primary photons but also from every Standard Model particle with mass $m < 1$ GeV. We have used Equation 3.5 from [Carr et al. (2010)] and the degrees of freedom associated to every particle involved, which are gluons, photons, leptons and the three lightest quarks, to weight the contributions from every particles species.

Figure 4 shows our primary emission spectrum and our final reemission spectrum. The normalization of the final reemission one is defined so that

$$\int_{E_1}^{E_2} E\frac{d^2N_\gamma^{(2)}}{dEdt} = \sum_s f_s \int_{E_1}^{E_2} E\frac{d^2N_\gamma^{(1)}}{dEdt} \tag{25}$$

where (1) and (2) distinguish between the primary emission and the final reemission spectra and f_s is the weighting factor for every particle species, that depends on their spin. In other words, we make sure that the total emission power coming from the injected photons and other particles is invested in reemiting photons from the plasma. That is the normalization condition.

However, looking at the spectra profiles, we see that they are quite different from those published by Carr et al.. The most important reason is that we have assumed a thermal spectrum profile, especially given that our ultrarelativistic perfect fluid simplification does not consider any jet calculation. In the primary spectrum, we observe a pretty different slope before the peak, which has to do with the fact that we have considered our primary spectrum to be formed by the primary photons emitted directly from the BH at r_{BH} by Hawking-radiation, while Carr et al. have already considered contributions from particle species other than photons, and probably backscattering and other phenomena. In the final reemission

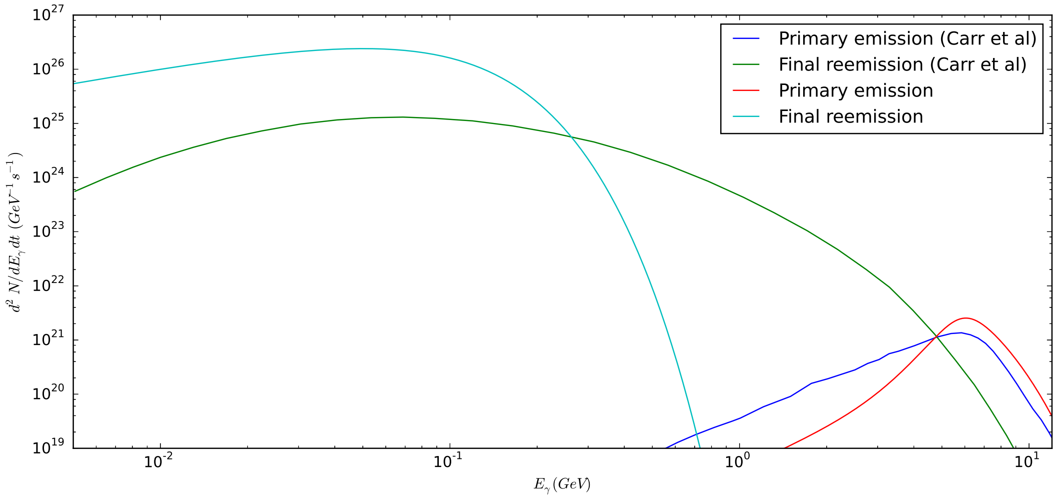

Figure 4: *Thermal spectra corresponding to our toy model. We plot our primary emission and final reemission profiles together with those of Carr et al. for comparison.*

profile, the most important change is the thermal assumption, because it drastically changes the behaviour after the peak. Since the suppression is much quicker and the normalization is given by an integral equation that corresponds to the area of the figure, it is easy to understand why we find a higher peak, even though at smaller energies our spectrum reaches higher values, because we then deal with energies that are 1 to 2 orders of magnitude lower and their contribution to the integral is much smaller.

We can see that this emission profile model seems plausible, but seems to differ significantly in some points from the more detailed model by Carr et al. and suggests a clear magnitude of the systematic error associated with the modelling of the emission spectra.

2.3 Constraint on Ω_{PBH}

The fact that we expect a higher emission rate around 68 MeV than Carr et al. has consequences regarding the Ω_{PBH} and the extragalactical gamma-ray background constraints. We will briefly discuss that as a final comment of this chapter.

According to [Carr et al. (2010)], if we approximate the number of emitted photons in a given logarithmic energy interval $\Delta E_\gamma \simeq E_\gamma$ by $\frac{dN_\gamma}{dt} \simeq E_\gamma \frac{d^2N_\gamma}{dEdt}$, we can express the emission rate per volume at cosmological time t as

$$\frac{dn_\gamma}{dt}(E_\gamma, t) \simeq n_{PBH}(t) E_\gamma \frac{d^2N_\gamma}{dE_\gamma dt}(M(t), E_\gamma) \tag{26}$$

where n_i stands for the number density of gamma-rays or PBHs, depending on the index i in the equation. Given that the emission rate per volume $\frac{dn_\gamma}{dt}$ is known from measurements (see Figure 4 of [Carr et al. (2010)]), variations in either n_{PBH} or $\frac{d^2N_\gamma}{dEdt}$ imply an inversely proportional change in the other factor to match the constraint imposed by the experimental results.

As we have seen in the results displayed in Figure 4, we have found a higher peak for $\frac{d^2N_\gamma}{dEdt}$ than Carr et al.. More precisely,

$$\left(\frac{d^2N_\gamma}{dEdt}\right)_{peak} \simeq \begin{cases} 1.30\times 10^{25}\mathrm{GeV}^{-1}\mathrm{s}^{-1} & \text{for Carr et al.} \\ 2.40\times 10^{26}\mathrm{GeV}^{-1}\mathrm{s}^{-1} & \text{for our spectrum} \end{cases} \tag{27}$$

Then, the ratio indicates an improvement of a factor

$$\frac{2.40\times 10^{26}}{1.30\times 10^{25}} = 18.39. \tag{28}$$

Given the experimental constraints we mentioned before, this change indicates that n_{PBH} should be 18.39 times smaller than the values found by Carr et al. and, as we can see in their paper, n_{PBH} can be related to Ω_{PBH} so that

$$\Omega_{PBH} \propto \beta \propto n_{PBH} \tag{29}$$

meaning that Ω_{PBH} should also be 18.39 smaller. Here $\beta(M)$ is the mass fraction of the Universe that corresponds to PBHs of intial mass M. Then, we find that, according to our toy model, the constraint on the PBH density parameter is given by

$$\Omega_{PBH} \leq \frac{5\times 10^{-10}}{18.39} = 2.72\times 10^{-11}. \tag{30}$$

3 Sensitivity to evaporating BHs with gamma-ray detectors

In the following pages, we present how we have determined the sensitivity to PBH bursts. The method is based on the assumption of a uniform distribution of PBHs and computes the minimum detectable burst rate density in the observed volume (defined by the MAGIC FOV and the maximum distance for detectable evaporating BHs) with a significance of 5 standard deviations.

In the previous chapter, we have seen that our model predicts an emission spectrum peaked around 68 MeV, which is way below the energy detection range of MAGIC. This is due to the presence of the chromosphere around the BH, which redistributes the total emitted flux to lower energies. It would not be possible to detect an object with such spectrum with MAGIC and, for this reason, we have considered another spectrum from a chromosphereless model.

3.1 Methodology

The method we present here is an adaptation of the one presented for Milagro and HAWC (Hight Altitude Water Cherenkov observatory) at [Abdo et al. (2014)], assuming the same expression for the gamma-ray spectrum but obviously considering the technical specifications of MAGIC to carry out the calculations.

As we have seen in Equation 5, we have an explicit relation between the temperature and the remaining lifetime of a BH. We have considered eight values for the remaining lifetime[2] τ, going from 10^{-3} s to 10^4 s. Given the mentioned expression, these correspond to eight different initial temperatures.

We consider a spectrum given by

$$\frac{dN}{dE} \approx 9\times 10^{35} \text{ photons GeV}^{-1} \begin{cases} \left(\frac{1\ GeV}{T}\right)^{3/2}\left(\frac{1\ GeV}{E}\right)^{3/2}, & E<T \\ \left(\frac{1\ GeV}{E}\right)^{3}, & E\geq T \end{cases} \tag{31}$$

shown in Figure 5 for several remaining lifetimes, given that the temperature is $T = T(\tau)$ (expressed in GeV).

The next step is to compute the number of detected photons by the MAGIC telescopes given their detection energy range, effective collection area and assuming a certain distance to a BH. The expected number of detected photons coming from an evaporating BH at distance r with remaining lifetime τ is given by

$$\mu(r,\tau) = \frac{1-f}{4\pi r^2}\int_{E_1}^{E_2} dE' \int_0^{\infty} dE \frac{dN(\tau)}{dE} A(E) G(E,E') \tag{32}$$

[2]Throughout this work, we will refer to τ as *remaining lifetime*, *observation time* of an event and *integration time window*. They are all equivalent, because the burst takes place when the BH is about to expire and this is the time interval of our interest.

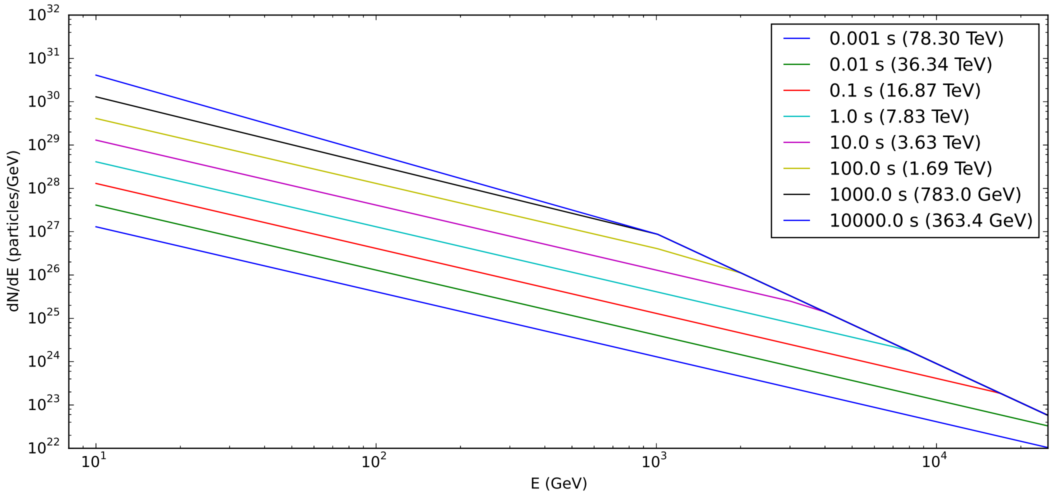

Figure 5: *Time-integrated spectrum from an evaporating BH for eight different values of* τ *(from* 10^{-3} *s to* 10^4 *s).*

where f is the dead time fraction of the detector, (E_1, E_2) is the integrated range of estimated energy, A is the effective area of the detectors, E is the true energy of the incoming gamma-ray, E' is the estimated energy value from the shower and G is the energy dispersion function, that describes the PDF of the energy estimator as a function of E, which can be approximated by a Gaussian characterized by an energy resolution and bias (both depending on E).

Notice that, to be able to evaluate this integral, we need to set a value for the distance r, as well as to determine certain technical specifications of the MAGIC telescopes. Let us do this first.

To obtain most of the technical information of the MAGIC detectors, we have used values, tables and plots from [Aleksić et al. (2014)]. Those correspond to the performance of the telescopes since 2012, when a major upgrade of the data acquisition electronics and the MAGIC-I camera was finished. To begin with, we have looked for the effective collection area A of the telescopes and selected the values for low zenith angles, for which most MAGIC observations are performed (see Figure 7 of [Aleksić et al. (2014)]). To be more precise, we have used several data points to interpolate and obtain a function for the full energy range. The result is shown in Figure 6. Notice that there are also some extrapolated values. Even though they are expected to be out of the MAGIC detection energy range, we will need them to perform some calculations later. For simplicity, we have assumed that at low energies the linear suppression (in logarithmic units) we can see in the figure continues. However, this is just a technical issue, neglectful from a conceptual point of view.

Taking a look at the integral equation we are trying to solve, the next function we need to define is the energy dispersion function G. As we have mentioned before, for a given value

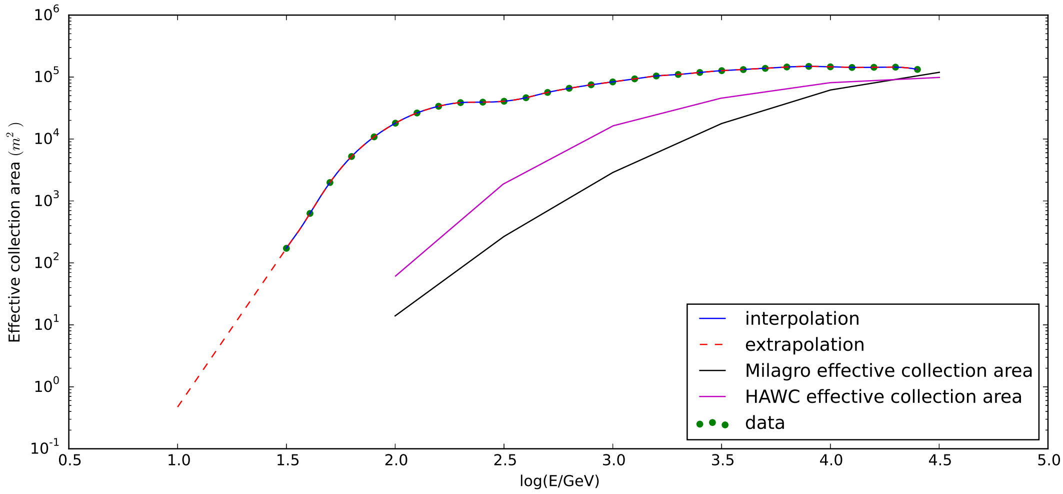

Figure 6: *Effective collection area of the MAGIC telescopes (after the upgrade) for low zenith angles. Those of Milagro (for zenith between 0° and 15°) and HAWC (for zenith between 0° and 26°) are shown for comparison.*

of the true energy E, this function can be approximated by

$$G(E,E') = \frac{1}{2\pi\sigma^2}\, \exp\left(-\frac{(E-E'+b)^2}{2\cdot\sigma^2}\right), \tag{33}$$

which is a Gaussian with mean value $E'-b$ and variance σ. Here b and σ are two parameters that are used to characterize the distribution, called energy bias and energy resolution, respectively. They actually depend on the true energy E and, once again, we have used the values that are presented in Figure 10 of [Aleksić et al. (2014)].

The procedure we have used to obtain these values is the same we have explained for the effective collection area before and, once again, aside from the interpolation from the data points, we have extrapolated to use values out of the MAGIC detection energy range in later calculations. The corresponding plot can be seen in Figure 7. Having set these values, we have fully determined the energy dispersion function G.

It is important to point out that the functions we have used for the effective collection area A and the energy dispersion G were not optimized for the search of PBHs, but for the detection of the Crab Nebula. The fact that it is a continuously emitting source with a totally different spectrum suggests that a taylored PBH analysis (with different A and G functions) could be envisaged. This optimization would be a natural continuation of this work.

We will now estimate the value of μ that allows a 5σ detection of a PBH over the cosmic background. This is what we will name μ_0, which through Equation 32 can be expressed as a maximum distance to the detectable source, r_{max}. To do so, we equate a Poisson probability

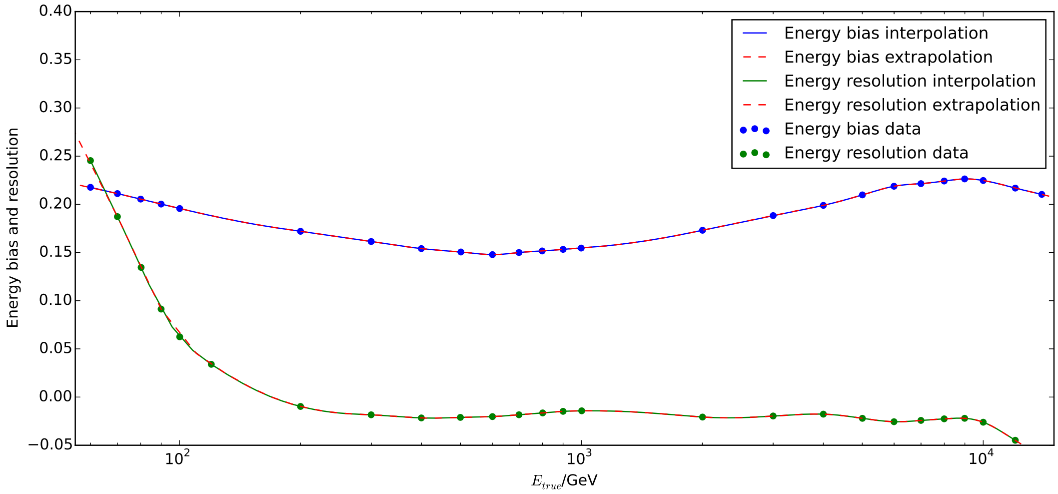

Figure 7: *Energy bias and energy resolution with respect to true energy values for MAGIC.*

P described by a number of counts n to a certain p-value p_c [Abdo et al. (2014)], so that

$$p_c = \frac{p_0}{N_t} = P(\geq n|n_{bk}). \tag{34}$$

Here, by $P(\geq n|n_{bk})$, we mean the probability to get n or more counts with a Poisson mean of n_{bk}, $p_0 = 2.3 \times 10^{-7}$ is a p-value corresponding to 5σ, N_t is the number of trials, given the number of temporal and spatial windows we use in our search, and p_c is the Bonferroni corrected p-value corresponding to 5σ and N_t.

The number of trials N_t can be expressed as

$$N_t(\tau) = k(\tau) \cdot \frac{S}{\tau} \cdot \left(\frac{\theta_{MAGIC}}{\theta_{PBH}}\right)^2 \tag{35}$$

where S is the total search duration, θ_{MAGIC} is the aperture angle that defines the field of view (FOV), θ_{PBH} is the aperture angle for a point-like source analysis (comparable to the angular resolution of the instrument) and $k(\tau)$ is a correction factor (<1) that accounts for the fact that for small τ, the burst may be detected in several time windows, and therefore not all trials are independent [Vasileiou (2008)]. The total search duration S is defined by the experiment and θ_{MAGIC} and θ_{PBH} have been considered to be 1° and 0.16°, respectively (looking at Figure 14 of [Aleksić et al. (2014)], we decided to consider an angular resolution of 0.16° as a very conservative approximation). Then, we only need to determine $k(\tau)$. We have used the published results by Abdo et al. to recover their values of k and use them. For τ values they had not considered, we have used $k = 1$. In terms of their results, the overlapping correction can be written as

$$k(\tau) = \frac{N_t \cdot \tau \cdot \theta^2_{PBH}}{S \cdot \theta^2_{HAWC}}. \tag{36}$$

Integration time window τ (s)	Overlapping correction k
10^{-3}	5.45×10^{-2}
10^{-2}	5.45×10^{-2}
10^{-1}	4.96×10^{-1}
1	4.96×10^{-1}
10	7.60×10^{-1}
10^{2}	7.60×10^{-1}
10^{3}	1
10^{4}	1

Table 3: *Values for the overlapping correction k we have used in our calculations of N_t for every integration time window τ value.*

In Table 17 of [Abdo et al. (2014)], they have published the values of N_t for each zenith angle band, and we also know that they considered a total search duration of 5 yr and aperture angles of $\theta_{PBH} = 0.7^\circ$ and θ_{HAWC} corresponding to a FOV of 1.8 sr. Then, we only need to introduce a certain value of τ to the expression to recover the corresponding value of k. Doing so, we find the results shown in Table 3. As mentioned before, for $\tau > 10^2$ s, we have assumed $k = 1$ (the most conservative choice) because we could not extract the value in the same way.

Going back to the determination of μ_0, given that p_0 is a fixed number and that N_t and n_{bk} only depend on the duration of the observation, which we can consider to be τ for any event, it is easy to determine a value for n from Equation 34 for every value of τ under consideration in this work. Then, μ_0 is defined so that

$$P(\geq n|(n_{bk} + \mu_0)) = 0.5. \tag{37}$$

That is, μ_0 is the number of events from an evaporating black hole such that it would produce a 5σ detection (after trial correction) 50% of the times.

Let us discuss the dead time fraction f. The dead time fraction is defined as

$$f = R \cdot t_d \tag{38}$$

where R is the event rate during the time interval of interest and t_d is the dead time of the detector after any trigger. For a typical MAGIC event: $R_{bk} \sim 300$ Hz (usually dominated by the charged cosmic ray rate), $t_d \sim 26$ μs (before the MAGIC update, $t_d \sim 500$ μs) and $f < 0.01$. However, this situation we deal with in this work might not exhibit a typical MAGIC event rate, because shortly before expiring, a BH is expected to be able to reach an emission rate so high that would surpass the typical one for MAGIC. We have considered the effective event rate to be

$$R = R_{PBH} + R_{bk} \tag{39}$$

where R_{PBH} is the PBH event rate. We have approximated the PBH event rate as $R_{PBH} = \frac{\mu_0}{\tau}$.

Figure 8 shows the different mentioned rates in order to see that in the particular case we consider, R_{PBH} is indeed larger than R_{bk} for small τ, ultimately changing the dead time

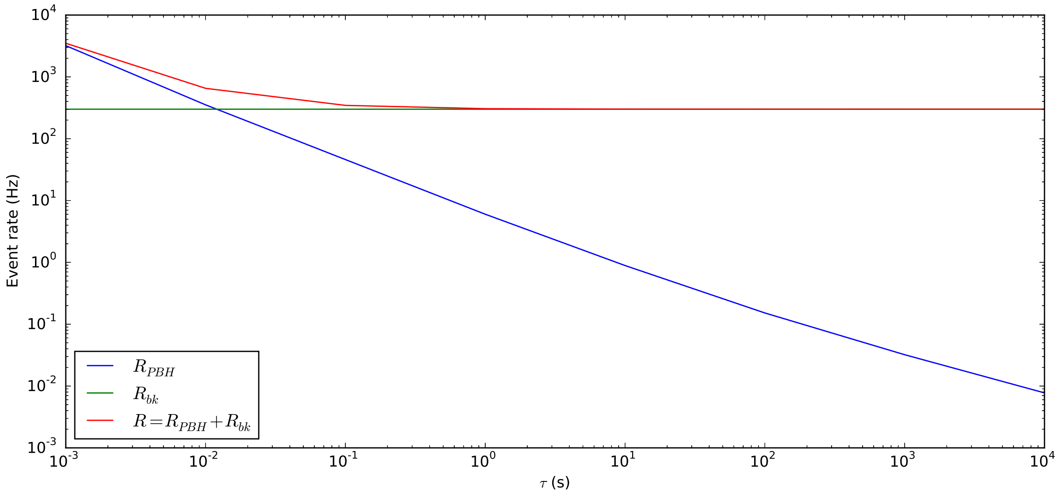

Figure 8: *Event rates for PBHs, typical MAGIC background rate and the total event rate considered in this study as a function of the integrated time window τ.*

Integration time window τ (s)	Dead time fraction f
10^{-3}	9.10×10^{-2}
10^{-2}	1.70×10^{-2}
10^{-1}	9.00×10^{-3}
1	7.96×10^{-3}
10	7.82×10^{-3}
10^{2}	7.80×10^{-3}
10^{3}	7.80×10^{-3}
10^{4}	7.80×10^{-3}

Table 4: *Dead time fraction value for every integration time window considered in this work.*

fraction for these integration time windows by up to more than a factor of 10. In Table 4 we can see the values we dead time fraction values we find using this definition of the event rate R.

From Equation 32 we can easily see that

$$r_{max}(\tau) = \sqrt{\frac{1-f}{4\pi\mu_0(\tau)} \int_{E_1}^{E_2} dE' \int_0^{\infty} dE \frac{dN(\tau)}{dE} A(E)G(E,E')} \tag{40}$$

allows to find the maximum distance where we can see the source at 5σ.

Assuming that a source can be seen from any point within the MAGIC field of view up to a distance of r_{max}, the effective volume where we can see a source with our detector can be expressed as

$$V(\tau) = \frac{4\pi}{3} r_{max}^3(\tau) \cdot \frac{FOV_{MAGIC}}{4\pi} = \frac{2}{3}\pi(1-\cos(1^\circ))r_{max}^3(\tau). \tag{41}$$

Following the method presented by Abdo et al. once again, we see that, assuming a uniform distribution of PBHs in the solar neighborhood, the 99% confidence level minimum detectable burst rate density of PBHs (i.e. the PBH burst sensitivity), which is the number of bursts per unit volume and unit time, can be written as

$$UL_{99} = \frac{4.6}{VS} \tag{42}$$

where 4.6 is a number that comes from the selection of a 99% confidence level (given that $P(n=0|4.6) = 0.01$), V is the effective detectable volume and S is the total search duration. Given that $V = V(\tau)$ and the search duration depends on the experiment under consideration, we can find sensitivity to PBH bursts for every value of τ we have considered.

So far in this section we have presented our method for a given estimated energy range (E_1, E_2). As long as we select an energy range for which we have the MAGIC technical data required, we can adjust E_1 and E_2 to find the interval of optimum sensitivity. The constraint on the possible intervals comes from the n_{bk} values we extracted from [Aleksić et al. (2014)], bacause the background event rates are given in certain energy intervals and hence we were forced to use the same ones. The whole possible range goes from 63 GeV to 10 TeV, but we have decided to consider energies from 158 GeV to 10 TeV because we still have most of the energy range available to MAGIC while supressing the two major contributions to the background noise, which happen to be between 63 GeV and 158 GeV, according to the background rates published at [Aleksić et al. (2014)]. The ideal thing to do would be to optimize our code to simultaneously look for the optimum time integration window τ and estimated energy range (E_1, E_2), but this has not been included in this work. However, we think this is a necessary step towards planning a search with MAGIC data.

3.2 Results for MAGIC

The method we have presented in the previous section is not exclusive for MAGIC. In fact, as mentioned in the beginning of this chapter, it is just an adaptation to MAGIC from a method used in [Abdo et al. (2014)] for Milagro and HAWC. In principle, similar adaptations could be done to use the same method with other experimental facilities in order to determine their sensitivity to the PBH burst rate density. In the next section, we will detail some differences between our model and that of Abdo et al. while comparing results.

To begin with, it is important to point out that these are not experimental results using the MAGIC telescopes, meaning that no data have been used to obtain them. This study is aimed to evaluate the capabilities of MAGIC in the field of PBH burst detection by determining the MAGIC sensitivity to such events. As we have seen when we presented the method, these results are based on several technical and performance properties of the MAGIC telescopes that allow to estimate their capabilities, and this is all that was used in this work.

τ (s)	n_{bk}	N_t	μ_0	r_{max} (pc)	V (pc^3)	Sensitivity ($pc^{-3}yr^{-1}$)
10^{-3}	1.10×10^{-5}	7.67×10^{10}	3.20	0.094	2.67×10^{-7}	1.51×10^{7}
10^{-2}	1.10×10^{-4}	7.67×10^{9}	3.53	0.17	1.46×10^{-6}	2.77×10^{6}
0.1	1.10×10^{-3}	6.97×10^{9}	4.60	0.26	5.58×10^{-6}	7.22×10^{5}
1	1.10×10^{-2}	6.97×10^{8}	6.01	0.40	2.10×10^{-5}	1.92×10^{5}
10	0.11	1.07×10^{8}	8.89	0.57	5.91×10^{-5}	6.82×10^{4}
10^{2}	1.1	1.07×10^{7}	15.2	0.71	1.15×10^{-4}	3.52×10^{4}
10^{3}	**1.1**	**1.41×10^{6}**	**32.1**	**0.75**	**1.37×10^{-4}**	**2.94×10^{4}**
10^{4}	11	1.41×10^{5}	77.5	0.69	1.05×10^{-4}	3.82×10^{4}

Table 5: *Results for MAGIC showing several magnitudes calculated throughout the process to estimate the PBH burst sensitivity. We have assumed a total search duration of 10×1000 h (it only affects the sensitivity values, shown in the last column) and considered an energy range from 158 GeV to 10 TeV. The row corresponding to $\tau = 1000$ s is shown in bold letters because it is the case of best sensitivity of our study with MAGIC.*

Table 5 shows the results for MAGIC, not only regarding the PBH burst sensitivity, but also the values of certain key magnitudes in the estimation we present, namely n_{bk}, N_t, $\mu_0(\tau)$, $r_{max}(\tau)$ and $V(\tau)$, for every considered value of the integration time window τ, assuming a total search duration S of 10×1000 h (which affects only the sensitivity values) and considering an energy range going from 158 GeV to 10 TeV. We express S as (total number of observation years, in years)×(observation time per year, in hours) because the different facilities mentioned in this work present different observation times per year and separting both contributions to S allows a quicker and easier comparison. Notice that for the smallest integration time window, the sensitivity is very poor. That is due to the lack of photons reaching the detector in such a small time interval and the large number of trials. As the integration time window increases, the chances of photon detection increase as well, and hence it is normal to observe an improvement in our results. We see that we have a minimum in our sensitivity that corresponds to a integration time window of $\tau = 10^3$ s. This comes from the fact that for the predicted spectra (Figure 5), as τ increases, the number of collected gamma rays increases faster than the background fluctuations up to a point when the it does not pay off to enlarge the time window, because the number of extra collected photons (given the short duration of these flares) does not compensate for the extra integrated background. In addition to that, there is the decrease of N_t as τ increases. Keep in mind that the p-value, that imposes a condition on n and, ultimately, on μ_0, is inversely proportional to N_t. For this reason, the minimum exists where there is the best balance between a signal that is strong enough to be measured and a background noise low enough (in relation to the given p-value) to allow these measurements. The determination of the value of τ for which we reach the optimum sensitivity is one of the main results of this work, because the integration time window will be a key parameter to take into account when designing a PBH search method.

Figure 9 shows a plot of the PBH burst sensitivity (following Equation 42) as a function of integration time window τ. In addition to the values shown in the previous table, corre-

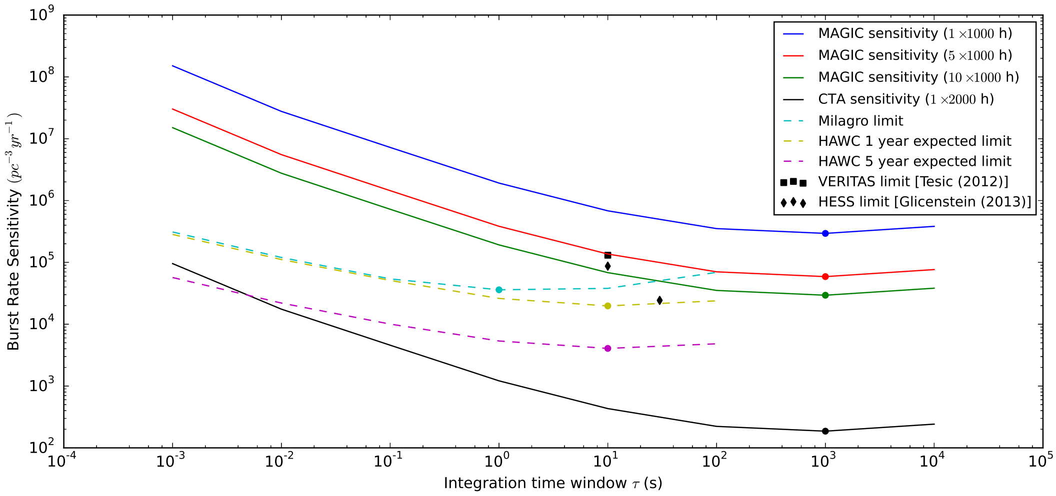

Figure 9: *PBH burst sensitivity estimated for MAGIC for several values of the total search duration S and an energy range considered to be* $(158\ GeV, 10\ TeV)$*. Milagro, VERITAS and HESS limits (in these cases, experimental data has been used) and HAWC expected limits are also displayed for comparison, as well as our estimation for CTA. The dots in each curve mark the optimum integration time window* τ *for each detector.*

sponding to a total search duration of 10×1000 h, we can see the values for $S = 1 \times 1000$ h and $S = 5 \times 1000$ h. Keep in mind that no MAGIC data has been taken into account to determine the sensitivity, meaning that these are just limits corresponding to a null detection hypothesis. In this case, we also considered an energy range going from 158 GeV to 10 TeV.

3.3 Milagro, HAWC and MAGIC

Let us now compare our results for MAGIC with those for Milagro and HAWC. The first thing we need to do when approaching this comparison is to point out the differences between the different experimental facilities that could affect the results. The first one we come up with is the fact the Milagro and HAWC are water Cherenkov radiation detectors[3], while MAGIC is a Cherenkov telescope. This is a major difference in the detection principle and, for example, has a dramatic effect in the observation time per year of these facilities. MAGIC can only observe at night and can achieve about 1000 h of observation time per year, while Milagro and HAWC could ideally observe twenty-four seven.

The effective collection area of MAGIC, shown in Figure 6, is very different to those of Milagro and HAWC at low energies (around 100 GeV), with the MAGIC one being up to 3

[3]A water Cherenkov detector is an array of water-filled tanks that contain PMTs to collect Cherenkov light produced by charged particles entering the detector volume. It can operate twenty-four seven, not being restricted by light as a Cherenkov telescope, and detect gamma-rays coming from any direction. The difference in arrival time in multiple tanks allows to determine the direction of the incoming particle.

τ (s)	HAWC background counts n_{bk}	MAGIC bacground counts n_{bk}
10^{-3}	6.37×10^{-2}	1.10×10^{-5}
10^{-2}	0.6372	1.10×10^{-4}
0.1	0.1355	1.10×10^{-3}
1	1.0481	1.10×10^{-2}
10	2.4405	0.11
10^{2}	24.4049	1.1
10^{3}	-	11
10^{4}	-	110

Table 6: *Number of background counts in a burst of duration τ for HAWC and MAGIC, considering all possible τ values studied.*

orders of magnitud larger. They are, however, pretty similar at large energies (10 TeV and higher).

The detected background noise is also different, and this has a direct effect on the results, because the determination of n and μ_0 strongly depend on that. Table 6 shows the expected number of background counts in a burst of duration τ for HAWC and MAGIC. Notice that we are not only comparing values for different experimental facilites, but also that they correspond to different energy intervals, HAWC having an optimum sensitivity around 1 TeV and MAGIC around 100 GeV. However, the two major causes of the difference we observe are that HAWC has an angular resolution around 0.7° while MAGIC's one is 0.16° and also that IACTs are intrinsically better at distinguishing between gamma-rays and background than water Cherenkov detectors, which means that, for similar effective collection areas, HAWC will have more background noise than MAGIC. As the reader might have noticed, n_{bk} values for MAGIC scale up linearly with τ, while this is not the case for HAWC. We assume that Abdo et al. must have optimized their method so that it performs at its best for every value of the integration time window, and this is something we have not performed in this work for MAGIC. Our first approach to the matter is not case-optimized, leaving a simpler dependence on τ, meaning also that there is still room for improvement in that regard.

Regarding the metholody we have used, there are a couple of differences we want to point out. In the calculation of the integral in Equation 32 we have convoluted the gamma-ray spectrum with the energy dispersion function (G) before integrating over estimated energy E'. According to [Abdo et al. (2014)], this is not what has been done for Milagro and HAWC. A quick look at Equation 3 of the mentioned paper shows that only one integral is performed and that the energy dispersion function is not considered. This is fine as long as they include all detected events irrespective of their estimated energy, but we consider it to be one of the most important parts of the adaptation of the method to MAGIC because it accounts for the energy reconstruction process that takes place when a MAGIC event is observed and allows for the optimization of the energy range in a future extension of this work.

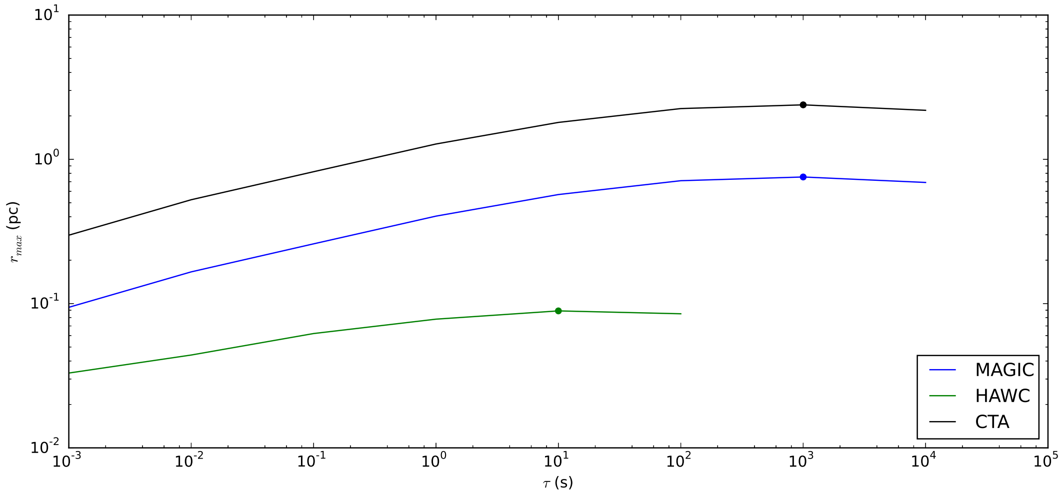

Figure 10: *Values for r_{max} for all the considered integration time windows for HAWC, MAGIC and CTA. The dots in each curve mark the maximum distance achieved by each detector.*

Before getting to the results of the PBH burst rate density, let us take a look at the values we have obtained for r_{max} for MAGIC and compare with those found by Abdo et al. for HAWC. We can find them at Table 7 and they are also displayed in Figure 10 for an easier comparison. We can see that, for optimum τ, the radius we find for MAGIC is almost 10 times larger (values shown in bold letters), meaning that MAGIC allows to observe at much larger distances than HAWC. However, the volume is slightly larger for HAWC because its FOV is much wider. MAGIC has a FOV of $2\pi(1-\cos(1^{\circ})) = 9.57\times10^{-4}$ sr, while HAWC's is $2\pi(1-\cos(26^{\circ})) = 0.64$ sr for the results we are considering. The real advantage of HAWC with respect to MAGIC is the much larger observation time per year.

Finally, having all these differences in mind, we get to compare the obtained values for the PBH burst sensitivity, which can be seen in Table 8. The first thing we can see is that every single value is smaller for HAWC than for Milagro or MAGIC, regardless of the integration time window we consider. We relate that to the fact that HAWC has shown larger effective volumes (for almost every case for which we have HAWC results) and observation times per year than MAGIC. We lack information regarding how the limits for Milagro have been calculated, namely the energy range, the observation time per year as well as the obtained values for r_{max}. We do know, though, that Milagro is similar to HAWC with a worse effective collection area, so results are expected to be worse. We also see, taking a look at Figure 9, that the limits for Milagro and HAWC exhibit a similar steepness in their dependence on τ, while results for MAGIC vary more rapidly. We also find that the optimum integration time window for the different facilities is different: for Milagro, $\tau = 1$ s; for HAWC, $\tau = 10$ s; and for MAGIC, $\tau = 1000$ s.

In the same figure, we can see that limits for VERITAS and HESS (two IACTs) are

	HAWC		MAGIC	
τ (s)	r_{max} (pc)	V (pc^3)	r_{max} (pc)	V (pc^3)
10^{-3}	0.033	1.6×10^{-5}	0.094	2.67×10^{-7}
10^{-2}	0.044	4.2×10^{-5}	0.17	1.46×10^{-6}
0.1	0.062	9.2×10^{-5}	0.26	5.58×10^{-6}
1	0.078	1.72×10^{-4}	0.40	2.10×10^{-5}
10	**0.089**	$\mathbf{2.27 \times 10^{-4}}$	0.57	5.91×10^{-5}
10^2	0.085	1.91×10^{-4}	0.71	1.15×10^{-4}
10^3			**0.75**	$\mathbf{1.37 \times 10^{-4}}$
10^4			0.69	1.05×10^{-4}

Table 7: *Values of r_{max} and V published at [Abdo et al. (2014)] for HAWC and our results for MAGIC. Values shown in bold letters are the optimum ones for each facility.*

τ (s)	Milagro	HAWC	MAGIC
10^{-3}	3.1×10^5	5.69×10^4	1.51×10^7
10^{-2}	1.2×10^5	2.20×10^4	2.77×10^6
0.1	5.4×10^4	1.00×10^4	7.22×10^5
1	$\mathbf{3.6 \times 10^4}$	5.35×10^3	1.92×10^5
10	3.8×10^4	$\mathbf{4.06 \times 10^3}$	6.82×10^4
10^2	6.9×10^4	4.82×10^3	3.52×10^4
10^3	-	-	$\mathbf{2.94 \times 10^4}$
10^4	-	-	3.82×10^4

Table 8: *PBH burst sensitivity found for Milagro, HAWC and MAGIC for all considered integration time window τ values. Values shown in bold letters are the optimum sensitivity values for each facility.*

also displayed for comparison. Even though their results are not discussed in this work, we reference [Tešić (2012)] and [Glicenstein (2013)] and show these values to get a quick idea about how other IACTs are doing in the field. We can also see our results for CTA (see Section 3.4).

It is important that we keep in mind all the differences we have mentioned between the facilities. Most importantly, we are not really observing the same region in the sky, which is relevant if, as expected, the PBH are not to be homogeneously and isotropically distributed around the Earth.

Our conclusion of the comparison is that the sensitivity values are not the only relevant quantity to take into account, because, even though they are not the same for all the facilities, they are certainly comparable. It has to be stressed that very different regions in the sky are being observed with MAGIC with respect to HAWC (as we said, we lack information to compare in detail with Milagro). On top of that, MAGIC has been operating for 11 yr, so there are plenty of data to carry out a search, which would be a natural continuation of this work, whereas HAWC is now starting its operations.

According to this work, even though it is not fully optimized to the search of PBHs, we see that, in a conical volume defined by a maximum distance[4] of 0.75 pc and a FOV with a radius of 1°, we expect the MAGIC telescopes to have a large enough sensitivity to allow a 5σ PBH detection if the local PBH burst rate density is 2.94×10^4 pc^{-3} yr^{-1} or larger.

3.4 Brief approach to CTA

The Cherenkov Telescope Array (CTA) is a planned observatory with two arrays of IACTs, one in each hemisphere, covering an energy range from a few tens of GeV to around 100 TeV. Construction will start by the beginning of 2016 in sites in Chile and La Palma (Spain). CTA is expected to surpass the flux sensibility of the current IACTs such as MAGIC, HESS or VERITAS by an order of magnitude. We have run our code for MAGIC changing a couple of parameters to adjust to the values of CTA, namely the value of

$$\int_{E_1}^{E_2} dE' \int_0^\infty dE \frac{d^2N}{dEdt} A(E) G(E,E'), \tag{43}$$

which we expect to be $\sim$10 times bigger for similar background rate because of the increased flux sensibility, the FOV of the detector, which we will assume to have a radius of 5° (there are different telescopes in each hemisphere, but we will consider they reach 5° on average) and the observation time per year, which we will consider to be two times that of MAGIC given that we observe with two observatories.

These changes cause the values of $r_{max}(\tau)$ and $V(\tau)$ to differ significantly from those found for MAGIC. As a consequence, the sensitivity values we find are also significantly better. Notice that the factor 10 improvement in sensitivity increases the values of r_{max} by a factor $\sqrt{10}$, and the change in FOV causes an increase in V of a factor $\sim$25 in addition to the

[4]The closest star to the Sun is Proxima Centary, about 1.3 pc away.

Integration time window τ (s)	$r_{max}(\tau)$ (pc)	$V(\tau)$ (pc^3)	Sensitivity (pc^{-3} yr^{-1})
10^{-3}	0.30	2.11×10^{-4}	9.54×10^{4}
10^{-2}	0.52	1.15×10^{-3}	1.75×10^{3}
0.1	0.82	4.40×10^{-3}	4.57×10^{3}
1	1.28	1.67×10^{-2}	1.21×10^{3}
10	1.80	4.67×10^{-2}	4.31×10^{2}
10^{2}	2.25	9.05×10^{-2}	2.22×10^{2}
10^{3}	**2.39**	**0.11**	**1.86×10^{2}**
10^{4}	2.19	8.33×10^{-2}	2.41×10^{2}

Table 9: *Sensitivity for CTA, as well as values for the two magnitudes that significally change in our adaptation of the MAGIC code to CTA. Values shown in bold letters correspond to the optimum sensitivity.*

factor $10^{3/2}$ coming from r_{max}^3 for a total increase factor of $\sim$790. Regarding the sensitivity, the improvement is of a factor $\sim$1580 coming from the $(V \cdot S)^{-1}$ dependence. It is important to mention, though, that in this approximation we are assuming that N_t does not change, which is not true. Therefore, the results presented here must be regarded with care and as a first estimation of the order-of-magnitude sensitivity of CTA in PBH searches.

In Table 9 we can see the results we obtain with this simple estimation and the sensitivity is also displayed in Figure 9 together with the rest of the sensitivity values discussed in this work for comparison. For all these calculations, we have considered a total search duration of $S = 1 \times 2000$ h and an estimated energy range going from 158 GeV to 10 TeV, given that this estimation for CTA is just a simple adaptation of our calculations for MAGIC. It is easy to understand the huge improvement we can see in the figure if we take a look at the massive radii we obtain, reaching beyond 2 pc, as well as the enormous volumes we would be able to observe, in comparison to MAGIC or HAWC.

The conclusion of this brief approach to CTA is that the expectations are that CTA could reach sensitivities well below those of MAGIC or HAWC after the first year of operations, being by far the best candidate to carry out a PBH search in the TeV range.

4 Conclusions and outlook

In this work, I have approached two of the most important aspects related to the search for PBHs, which are the determination of the expected particle emission spectrum and the perspectives for detection with the present and future gamma-ray instruments. On one hand, I have presented a simple toy model for PBH chromospheres and emission spectra. The main assumptions are that, as a first approximation, the chromosphere can be treated as an ultrarelativistic perfect fluid with equation of state very similar to that of radiation (i.e. $w = 1/3$) and that the emission spectrum behaves as a thermal one with its peak around $m_{\pi_0}/2 = 68$ MeV. On the other hand, I have explained an adaptation for MAGIC of a method, that Abdo et al. originally applied to HAWC, to calculate the MAGIC sensitivity to PBH bursts. The main variations with respect to the original method are the consideration of MAGIC technical and performance properties instead of those of HAWC, a new approach to the determination of the event rate R and the inclusion of the energy dispersion function G, that accounts for the energy reconstruction process of MAGIC.

I have checked that the chromosphere toy model is physically plausible, even though we do not expect a chromosphere to behave exactly like an ultrarelativistic perfect fluid. It is remarkable that such a simple model already resembles significantly the outcome of the much more contrived models based on jet algorithms.

The thermal spectrum assumption leads to a spectrum with a few differences when compared to that of a more involved and detailed method like that of Carr et al.. The emission spectrum shows a stronger dependence on energy before the peak in our model, while there is a much quicker suppression after the final reemission peak. Since Carr et al. consider phenomena such as backscatering and jet quenching, we interprete these differences as a consequence of our simplification of QCD calculations. The most important consequence of this is that the 68 MeV final reemission peak is one order of magnitude higher in our model, which leads to the discussion on Ω_{PBH} constraints. A higher peak energy results in a tighter constraint for Ω_{PBH} in order to fulfil the condition imposed by experimental measurements of the gamma-ray background. The constraint I find is more stringent by around one order of magnitude,

$$\Omega_{PBH} \leq 2.72 \times 10^{-11}. \tag{44}$$

I also notice that, if spectra were so soft as in our toy model, facilities such as MAGIC and CTA would experience a dramatic loss in sensitivity in comparison to the values found in this work. However, even in the context of our model, it could be interesting to study the emission spectra for several initial temperatures to see how the spectra vary as the BH initial mass changes. Given the exponential suppression of the spectra at high energies, I think it is unlikely that a sizeable amount of particles reach the energy detection range of MAGIC or CTA, but it still would allow to rule out this possibility.

Regarding the methology to calculate the sensitivity to PBH bursts, I have included the energy dispersion function to account for the energy reconstruction process which allows for an optimization of the integrated energy range. I have also used a different way to calculate the event rate $R = R(\tau)$, which consists in adding the typical MAGIC event rate and the estimated one for PBHs for a given integration time window. Also related to the methodology is the fact that the effective collection area and the energy dispersion functions used in this work are optimized to observe the Crab Nebula. An optimization to the search of PBH bursts should be done, as well as designing a data selection method to distinguish a PBH burst from GRBs from other sources and another one to simulaneously optimize the integration time window and estimated energy range of the search. A similar approach should be taken with CTA, rather than adapting a few factors within the MAGIC method. Ideally, all these steps should be carried out from scratch independently for both facilities.

Results for MAGIC and Milagro present similar sensitivity values, while HAWC seems to do better than them by an order of magnitude given its slightly larger effective volume and, in particular, its longer duty cycle. However, the sensitivity found for MAGIC corresponds to a very different region in the sky, because it allows observation in a conical volume defined by an angle of 1° and a maximum distance of 0.75 pc, at optimum τ, compared to the $26^\circ \times 0.089$ pc volume of HAWC. On top of that, as I mentioned in the previous paragraph, there is plenty of room for improvement for MAGIC due to the multiple things that could be optimized in our method. With the method presented in this work, we find that MAGIC has a sensitivity of

$$2.94 \times 10^4 \text{ pc}^{-3} \text{ yr}^{-1} \tag{45}$$

for $\tau = 1000$ s, considering an estimated energy range from 158 GeV to 10 TeV and a total search duration of 10×1000 h.

CTA appears to be the most promising facility of those considered in this work, with expectations to present the lowest sensitivity, exploring the largest volume and doing so in regions farther away from Earth than any other detector. A fast estimation based on our results for MAGIC leads to an estimation for CTA that presents $\tau = 1000$ s as the optimum integration time window in the estimated energy range we considered, (158 GeV, 10 TeV), with a total search duration of 1×2000 h. In these conditions, the sensitivity of CTA is expected to be

$$187 \text{ pc}^{-3} \text{ yr}^{-1}. \tag{46}$$

A continuation of this work would make perfect sense for both MAGIC and CTA. On one hand, I have shown that MAGIC is expected to have a sensitivity comparable to that of Milagro and the amounts of data collected over the years would allow a search of PBH bursts, once the method is optimized and a data selection method has been designed. On the other hand, CTA is expected to be remarkably more sensitive than MAGIC, meaning that developing the required methods for a search would be key to look for PBH bursts within the energy range CTA covers with unprecedented sensitivity when enough data are collected.

References

[Aamodt (2011)] Aamodt, K. et al., *Suppression of Charged Particle Production at Large Transverse Momentum in Central Pb–Pb Collisions at* $\sqrt{s_{NN}} = 2.76$ *TeV*, volume B696, pages 30-39, Phys. Lett., 2011.

[Abdo et al. (2014)] Abdo, A. A. et al., *Milagro limits and HAWC sensitivity for the rate-density of evaporating primordial black holes*, volume 64, pages 4-12, Astropart. Phys., 2014.

[Aleksić et al. (2014)] Aleksić, J. et al., *The major upgrade of the MAGIC telescopes, Part II: The achieved physics performance using the Crab Nebula observations*, volume 72, pages 76-94, Astropart. Phys., 2016. Arxiv: 1409.5594v3.

[Carr et al. (2010)] Carr, B. J. et al, *New cosmological constraints on primordial black holes*, volume 82, issue 10, id 104019, Physical Review D, 2010.

[d'Enterria (2005)] d'Enterria, David G., *High p(T) leading hadron suppression in nuclear collisions at s(NN)**(1/2) = 20-GeV - 200-GeV: Data versus parton energy loss models*, volume C43, pages 295-302, Eur. Phys. J., 2005.

[Glicenstein (2013)] Glicenstein, J. et al., *Limits on Primordial Black Hole evaporation with the H.E.S.S. array of Cherenkov telescopes*, ArVix e-prints, 2013.

[Hawking (1971)] Hawking, S. W., *Gravitationally collapsed objects of very low mass*, volume 152, pages 75-78, MNRAS, 1999.

[Hillas (1985)] Hillas, A. M., *Cherenkov light images of EAS produced by primary gamma showers*, Proc. of the 19th ICRC, 1985.

[Hillas (2013)] Hillas, A. M., *Evolution of ground-based gamma-ray astronomy from the early days to the Cherenkov Telescope Array*, Astroparticle Physics, 2013.

[MacGibbon et al. (2008)] MacGibbon, J. and Carr, Bernard J. and Page, Don N., *Do Evaporating Black Holes Form Photospheres?*, volume D78, Phys. Rev., 2008.

[MacGibbon (2014)] MacGibbon, J. et al., *Primordial black holes*, 5th Fermi Symposium, 2014.

[Mukhanov and Winitzki (2004)] Mukhanov, V. F. and Winitzki, S., *Introduction to quantum fields in classical backgrounds*, Lecture notes, 2004.

[Page (1976)] Page, Don N., *Particle emission rates from a black hole: Massless particles from an uncharged, nonrotating hole*, volume 13, issue 2, Physical Review D, 1976.

[Page and Hawking (1976)] Page, D. N. and Hawking, S. W., *Gamma rays from primordial black holes*, volume 206, pt. 1, pages 1-7, Astrophysical Journal, 1976.

[Panov (2007)] Panov, Alexander D. et al., *The results of ATIC-2 experiment for elemental spectra of cosmic rays*, volume 71, pages 494-497, Bull. Russ. Acad. Sci. Phys., 2007.

[Tešić (2012)] Tešić, G. and VERITAS Collaboration, *Searching for primordial black holes with the VERITAS gamma-ray experiment*, Journal of Physics Conference Series, vol. 375, p. 052024, July 2012.

[Vasileiou (2008)] Vasileiou, V., *A search for bursts of very high energy gamma-rays with Milagro*, PhD thesis, University of Maryland, College Park, 2008.

[Weekes (1989)] Weekes, T. C. and Cawley, M. F. and Fegan, D. J., *Observation of TeV Gamma-rays from the Crab-Nebula Using the Atmospheric Cerenkov Imaging Technique*, The Astrophysics Journal, 1989.